Available online at www.sciencedirect.com
ScienceDirect
Continental Shelf Research 26 (2006) 2433–2453
CONTINENTAL SHELF RESEARCH
www.elsevier.com/locate/csr

Comparison of radiometric quantities measured in water, above water and derived from seaWiFS imagery in the South Atlantic Bight, North Carolina, USA

Piotr Kowalczuk[a,b,*], Michael J. Durako[a], William J. Cooper[a,1], David Wells[a], Jason J. Souza[a]

[a]*Center for Marine Science, The University of North Carolina Wilmington, 5600 Marvin Moss Lane, Wilmington, NC 28409, USA*
[b]*Marine Physics Department, Institute of Oceanology, Polish Academy of Sciences, ul. Powstańców Warszawy 55, PL-81-712, Sopot, Poland*

Received 19 August 2005; received in revised form 10 July 2006; accepted 17 July 2006
Available online 20 September 2006

Abstract

This paper reports on an ongoing study to better understand the bio-optical properties of a portion of the South Atlantic Bight—the Cape Fear River (CFR) plume area and Onslow Bay (OB). Sampling mid-Onslow Bay provides a contrasting coastal system relatively un-impacted by the high dissolved organic matter-waters of the CFR. Data were obtained during regular research-cruise observations, from October 2001 to September 2003, using two different measurement systems: above-water and in-water radiometers. Measurements were performed in marine and estuarine waters optically classified as Cases 1 and 2, respectively, and under variable atmospheric conditions. A statistical comparison of both approaches was conducted in support of the validation of remote sensing data from the *Sea*-viewing *Wi*de *F*ield-of-view *S*ensor (SeaWiFS) and local algorithm development. Remote sensing reflectance was calculated at four wavelengths 412, 443, 490, and 555 nm, and results from the two in situ approaches and SeaWiFS were compared. The spectrally averaged unbiased percent difference between remote sensing reflectance derived from the two field instruments was greater than, 25%, in the best case. Radiometric quantities derived from field measurements (e.g. diffuse attenuation coefficient at 490 nm and spectral remote sensing reflectance) were compared to available estimates from SeaWiFS images. The random mean square root error (RMSE) between field measurements and SeaWiFS estimates of the remote sensing reflectance ranged from 26.3% (at 555 nm) to 52.9% (at 412 nm). The RMSE between field measurement and SeaWiFS estimates of K_d 490 was 34.3%. Because the spatial scale of in situ measurements (meters) differ greatly from that of SeaWiFS (kilometers), sub-pixel variability in field measurements was investigated. Our results suggest that factors other than sub-pixel variability are responsible for observed discrepancies between in situ and satellite-based remote sensing reflectance.

*Corresponding author. Marine Physics Department, Institute of Oceanology, Polish Academy of Sciences, ul. Powstańców Warszawy 55, PL-81-712, Sopot, Poland. Tel.: +48 48 551 7281; fax: +48 58 551 21301.
E-mail address: piotr@iopan.gda.pl (P. Kowalczuk).
[1]Current address: Urban Water Research Center and Department of Civil and Environmental Engineering, University of California, Irvine, CA 92697-2175, USA.

0278-4343/$ - see front matter © 2006 Elsevier Ltd. All rights reserved.
doi:10.1016/j.csr.2006.07.024

1. Introduction

1.1. Theoretical background of ocean color observations

Remote observation of ocean color is a widely used method to study the distribution of various constituents of ocean waters (e.g. chlorophyll *a*), which can be used as indicators of phytoplankton productivity and biomass. The color of a water body (ocean) may be quantified by the apparent optical property (AOP) remote sensing reflectance (R_{rs}). Radiative transfer theory links R_{rs} with the inherent optical properties (IOP) of water (Mobley, 1994). The R_{rs} above the sea surface without sky reflection effects is proportional to the ratio of backscattering and sum of absorption and back scattering:

$$R_{rs}(\lambda) = \frac{L_W(\lambda)}{E_d(\lambda)} = \frac{ft}{Q(\lambda)n^2} \frac{b_b(\lambda)}{[a(\lambda) + b_b(\lambda)]}, \quad (1)$$

where $L_w(\lambda)$ is water leaving radiance, $E_d(\lambda)$, is downwelling irradiance, f is a proportionality factor depending on illumination condition and water optical properties determined by numerous modeling studies (Kirk, 1984; Gordon, 1989, Sathyendranath et al., 1989; Morel and Gentili, 1991) and equal to 0.32–0.33, t is the transmittance of the air–sea interface, $Q(\lambda)$ is the upwelling irradiance to radiance ratio $E_u(\lambda)/L_u(\lambda)$, n is the real part of the index of refraction of sea water, $b_b(\lambda)$ is the backscattering coefficient and $a(\lambda)$ is the absorption coefficient. In-water measurement of $R_{rs}(\lambda)$ is possible because there is little dependence on illumination conditions, i.e., the f/Q factor is relatively independent of solar zenith angle and wavelength (Morel and Gentili, 1993; Zibordi and Berthon, 2001). The ratio t/n^2 is approximately equal to 0.545 (where $n = 1.34$) and although it may change with the sea state, it is relatively independent of wavelength. The spectral shape of $R_{rs}(\lambda)$ is mostly determined by the shape of the absorption coefficient and the relative contributions of its constituents: absorption by pure sea water, $a_w(\lambda)$, absorption by chromophoric dissolved organic matter (CDOM), $a_{CDOM}(\lambda)$, and absorption by marine particles, $a_p(\lambda)$, which consists of the absorption by phytoplankton pigments, $a_{ph}(\lambda)$ and detritus, $a_d(\lambda)$. The magnitude of $R_{rs}(\lambda)$ is dependent on both: absorption level and on the value of backscattering coefficient which is the sum of the backscattering of pure sea water, $b_{bw}(\lambda)$, and backscattering by particles $b_{bp}(\lambda)$. In the clear central part of the ocean, absorption and backscattering of constituents of sea water, except water itself, may be simplified as a function of chlorophyll *a* concentrations (water optically classified as Case 1; Morel and Prieur, 1977), which enables the remote estimation of the chlorophyll *a* concentration on a global scale using empirical and semi-analytical algorithms (Gordon et al., 1983; Mitchell, 1994; Garver and Siegel, 1997; O'Reilly et al., 1998; O'Reilly et al., 2000; Maritorena et al., 2002). In coastal areas and semi-enclosed marine basins, which are under terrigenous influence, all backscattering and absorption components may change independently (waters optically classified as Case 2). The complex mutual relationships between the optically active components of sea water make their estimation by ocean color remote sensing algorithms very unreliable. Improvements to these algorithms may be achieved by empirical and semi-empirical modeling (Lee et al., 1998) of the IOPs in Case 2 waters, however, this work must be preceded by in situ collection of an IOP and AOP database.

Experimental determination of spectral remote sensing reflectance may be done in two ways: (1) by using in-water measurements extrapolated upward to calculate $R_{rs}(\lambda)$ above the water surface or (2) by taking above-water measurements. Alternatively, it is possible to measure $L_w(\lambda)$ just below the water surface from a floating platform (Froidefond and Ouillon, 2005). Both approaches have their advantages and limitations. In-water determination of $R_{rs}(\lambda)$ is done using a profiling radiometer which measures downwelling irradiance and upwelling radiance as a function of depth. From these vertical profiles, the diffuse attenuation coefficients of downwelling irradiance $[K_d(\lambda)]$ and upwelling radiance $[K_L(\lambda)]$ are calculated. Using these coefficients, the upwelling radiance values are propagated to just below the water surface by fitting an exponential model. Values for $E_d(\lambda)$ provided by a reference solar irradiance sensor were used in Eq. (1) to calculate $R_{rs}(\lambda)$ (Mueller and Austin, 1995). Sources of uncertainty for in-water spectral reflectance measurements include (1) ship shadow effects, which were minimized through the use of a free-fall instrument deployed from a small vessel; (2) sensor self-shadowing effects, which were minimized through the use of a slender profiler; and (3) accuracy of the depth sensor, which was addressed by adjusting the free fall velocity. Because

these are point measurements, acquired during oceanographic cruises in restricted time frames, additional uncertainty may be introduced by spatial variability.

Above-water measurements of spectral reflectance from a ship or fixed platform may be done accurately if specific instrument configurations and conditions are fulfilled. A set of radiometers for registering sky radiance, total reflected radiance and incident solar irradiance is required. In addition, a specific geometric setup of the instruments is needed (Mobley, 1999), the field of view should be very small, signal acquisition should be fast (Olszewski and Sokólski, 1990), and a specific algorithm for signal filtering to eliminate the radiance other than water-leaving radiance needs to be applied (Hooker et al., 2002). Following these conditions the remote sensing reflectance may be calculated from the equation:

$$Rrs(\lambda) = \frac{Lw(\lambda)}{Ed(\lambda)} = \frac{Lt(\lambda, \phi, \pi - \theta) - \rho Ls(\lambda, \phi, \theta)}{Ed(\lambda)}, \quad (2)$$

where $L_t(\lambda)$ is the total reflected radiance, $L_s(\lambda)$ is the incident sky radiance, ϕ is the azimuth angle, θ is the radiance incident angle, and ρ is the effective reflection coefficient depending on the measurement geometry and wind speed (Mobley, 1999). The approach presented above has been successfully tested in a series of experiments on a marine platform in the Adriatic Sea (Hooker et al., 2002; Zibordi et al., 2002). Above-water measurements of spectral reflectance can provide much better spatial and temporal coverage than in-water measurements because instruments can be mounted on various types of platforms: ships, low flying aircraft, satellites. However, serious methodological problems are associated with the above-water approach. Above-water measurements of $R_{rs}(\lambda)$ are very sensitive to illumination conditions (solar zenith angle, cloud cover), the angular distribution of upward radiance, sea state, position and stabilization of the instrument platform, and require an atmospheric correction, if the instruments are mounted on satellites or aircraft.

The aim of this paper is to compare the $R_{rs}(\lambda)$ measured in- , and above-water using two commercially available radiometer systems (Satlantic Inc.) during a series of cruises in the coastal ocean of the southeastern US. Secondarily, we aimed to test the interchangeability of in situ and above-water measurement methods in the study area and their applicability in SeaWiFS validation activities and the development of locally valid remote sensing algorithms for the retrieval of geophysical variables. Above-water measurements are also applied to the study of spatial variability of the upwelling radiance field at scales smaller than the 1-km scale of SeaWiFS pixels. Finally, SeaWiFS estimates of normalized water leaving radiance and diffuse attenuation coefficient K_d (490) are compared with ground-truth data collected in this highly variable coastal environment.

2. Methodology

2.1. Instrumental setup

This report describes a study period from October 2001 to September 2003. River-plume samples were collected from a sample grid developed for Coastal Ocean Research and Monitoring Program (CORMP) (see Fig. 1). This grid consists of seven stations (labeled CFP1 through CFP7) located at the Cape Fear River mouth and adjacent inner continental shelf. The grid was designed to study the spatial and temporal extent of the Cape Fear River plume. Onslow Bay samples were collected along a transect consisting of 14 stations (OB) starting at the sea buoy of Masonboro Inlet (station OBSB) and extending southeast across the continental shelf to its break at station OB63. The Cape Fear River plume area was sampled monthly (depending on weather) at ebb tide, for maximum extent of the plume. The Onslow Bay transect was sampled monthly in the 2001, and every second month from April 2002. Surface water samples were collected at all stations in the plume grid and at selected stations across Onslow Bay. Initially, water samples were collected at stations OBSB, OB15, OB27, OB42, OB57, OB63. After preliminary data analysis of the Onslow Bay data the sampling strategy was changed in April 2002, and samples were subsequently collected at every station from OBSB to OB27 to achieve better resolution of the near-shore spatial variability. All field operations were performed using small vessels: R/V Sturgeon (9 m) for the Cape Fear River plume and R/V Cape Fear (21 m) for Onslow Bay.

The radiometric measurements were conducted according to the SeaWiFS project protocol and its further revisions (Mueller and Austin, 1995; Fargion and Mueller, 2000) using a set of OCR-507 radiometers manufactured by Satlantic Inc.,

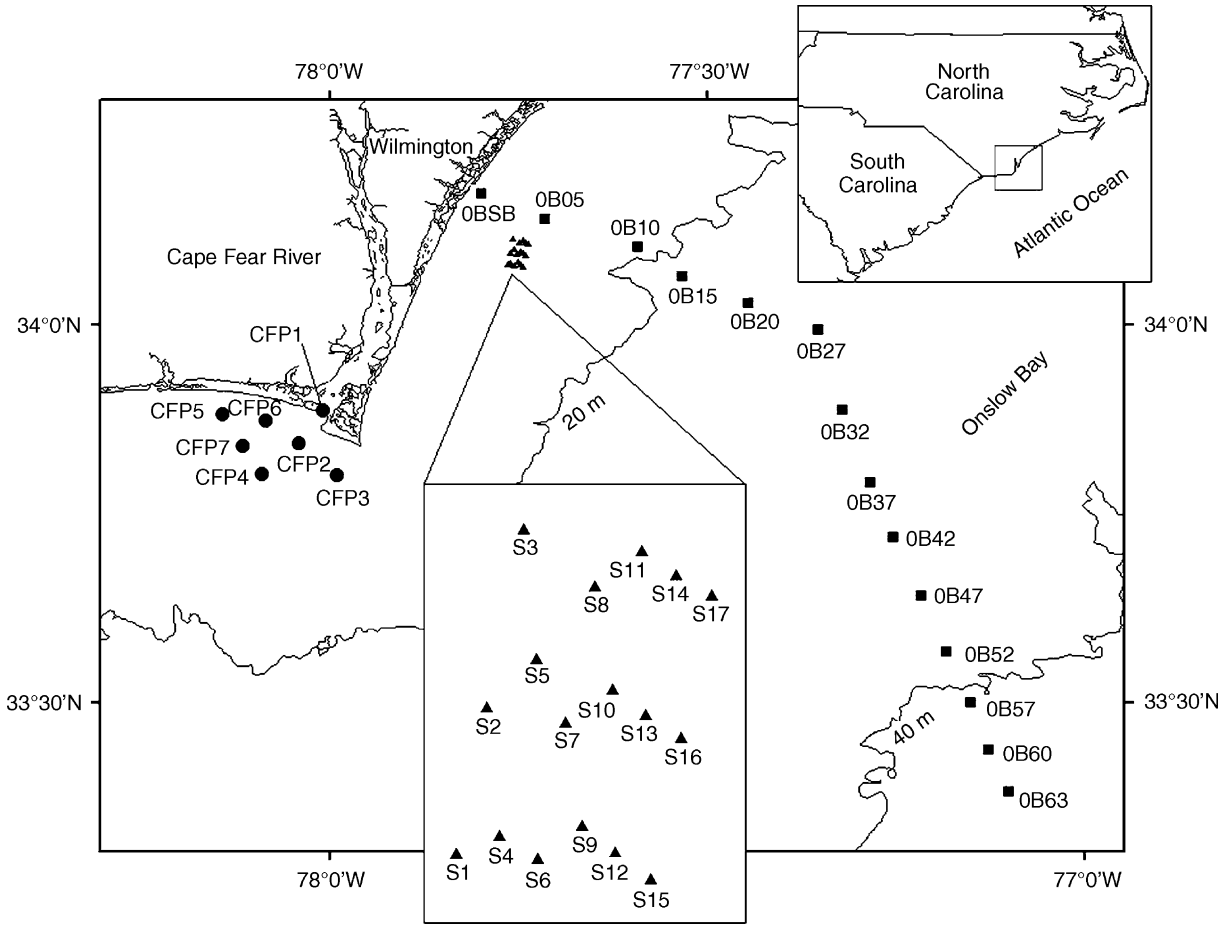

Fig. 1. Coastal Ocean Research and Monitoring Program (CORMP) sample station locations—Cape Fear River plume (CFP—circles), Onslow Bay (OB—squares) and sub-pixel variability cruise (S—triangles).

Canada. The geometrical setup of the radiometric instrument has been described by Hooker et al. (1999). Sensors were designed as follows:

1. A reference sensor to measure the incident solar irradiance at the ocean surface $E_s(0+, \lambda)$ at seven spectral bands: 412, 443, 490, 510, 555, 665, 865 nm. This was the reference sensor for both the profiling spectroradiometer and the above-water spectral reflectance meter.
2. An integrated sensor for measurements of downwelling irradiance $E_d(z, \lambda)$ and upwelling radiance $L_u(z, \lambda)$ at seven spectral bands: 412, 443, 490, 510, 555, 665, 865 nm, incorporated into a Satlantic MicroPro free-fall profiling vehicle. The viewing angle of the upwelling radiance sensor was 14°.
3. A set of two spectral radiance sensors to measure the total radiance reflected from the water surface $L_T(\lambda, \phi, \upsilon)$ and the indirect (sky) radiance $L_I(\lambda, \phi, \upsilon^1)$ at seven spectral bands: 412, 443, 490, 555, 665, 781, 865 nm, incorporated into a Satlantic MicroSAS base, which enabled control of both the azimuth and nadir angles. The viewing angle of both sky and total radiance sensors was 7°.

The reference sensor was mounted on top of the ship, above the superstructure. The MicroPro free-fall profiling vehicle was equipped with tilt, roll, temperature and pressure sensors and internal clock. Those sensors enabled the profiling vehicle to monitor inclination and descent speed, depth, and water column stratification during the cast. Data from tilt and roll, and pressure sensors were used as the quality control flags during data processing. All sensors were connected via telemetry cables to a notebook computer and 12 V battery.

SatView acquisition software provided by Satlantic Inc. read data from the MicroPro sensors to record depth profiles of $E_d(z, \lambda)$ and $L_u(z, \lambda)$ with simultaneous $E_s(0+, \lambda)$ readings, or from the MicroSAS radiance sensors measuring total and sky radiances with simultaneous $E_s(0+, \lambda)$ readings. The MicroPro profiling spectroradiometer was immersed on the sunny side of the ship's stern to minimize the shading effect of the research vessel. While at the surface, the pressure sensor was corrected for atmospheric pressure drift, the instrument was allowed to drift away from ship for a distance of approximately 10 m, then, released to free fall through the water column at 0.5–0.8 m s^{-1}. During descent, signals from the irradiance and radiance sensors were recorded. The MicroSAS base with sensors was deployed on the ship's midship gunnel. The nadir angle for the radiance sensor facing the sea surface was set up for $\upsilon = 40^\circ$ and the zenith angle for sensor facing the sky was equal $\upsilon^1 = \pi - \upsilon$· Mobley (1999) suggests pointing the radiometer at an angle of 135° relative to Sun's azimuth angle, and using a 90° azimuth angle if 135° cannot be reached. In practice, pointing the radiometer at 135° azimuth angle was almost impossible on the small research vessel constantly in motion. It was much easier to fix the instrument base perpendicular to ship and keep ship's stern positioned toward the sun, so the radiance sensors were positioned at an azimuth angle ϕ^1 within 90–110° relative to the sun's azimuth angle ϕ_s. Therefore, the nadir and zenith angles were chosen in close agreement with Mobley's (1999) recommendation. Signals from the sensors were collected for 3 min 10 s, which read approximately 1100 frames.

Raw sensor data were processed with Prosoft 6.3d processing software, developed and distributed by Satlantic Inc. The raw data were calibrated with calibration coefficients provided by the manufacturer, and then radiometric parameters were calculated, including spectral values of downwelling irradiance attenuation coefficient [$K_d(\lambda)$] spectral remote sensing reflectance [$R_{rs}(\lambda)$]. The quality of the data processing and radiometric quantity calculations were checked against the inclination and descent velocity signals. All data points with instrument inclination larger than 5° in both tilt and roll directions and descent speed over 0.5 m s^{-1} were eliminated from AOP calculations. Data from the MicroSAS instrument were calibrated and processed according to the procedure called S95 described by Hooker et al. (2002). Data were sorted according values of $L_T(865)$, then the mean value of the lowest 5% of the total readings for each waveband of $L_I(\lambda, \phi, \upsilon^1)$, $L_T(\lambda, \phi, \upsilon)$ and $E_s(0+, \lambda)$ were calculated. Sky glint was removed according to Eq. (2), where the mean value of ρ, the effective reflection coefficient, modeled by Mobley (1999) was equal to 0.028 for a wind speed range from 0 to 5 m s^{-1}.

The CDOM absorption coefficient at $\lambda = 350$ nm ($a_{CDOM}(350)$), spectral slope coefficient ($S_{300-500}$), were calculated from spectrophotometric scans of collected water samples, that were processed in the laboratory as described by Kowalczuk et al. (2003). Absorbance scans from 240 to 800 nm, 1 nm slit width, were made using 10 cm Suprasil cuvettes on a Cary 1E dual-beam spectrophotometer. Chlorophyll *a* concentration was calculated fluorometrically from 90% acetone extracts of particles retained on a fiber glass filter (GF/F) and measured on Turner AU-10 fluorometer, according to methodology by Welschmeyer (1994).

SeaWiFS Level 1A data were obtained from Goddard Space Flight Center for the following cruise dates: 24 October 2001, 22 January 2002, 17 April 2002, and 24 June 2002. Level 2 remote sensing products were derived using SEADAS version 4.1 with the standard global atmospheric correction algorithm and standard algorithms for calculation of remote sensing reflectance $R_{rs}(\lambda)$, and downwelling-irradiance diffuse-attenuation coefficient at $\lambda = 490$ nm, K_d (490). SeaWiFS estimates of radiometric quantities were then compared with in situ measurements.

2.2. Study area and ongoing monitoring program

The South Atlantic Bight (SAB), defined as the shoreline and continental shelf from Cape Hatteras to Cape Canaveral, is mostly coastal plain that grades gently into a wide (50–100 km) shelf. The wide shelf is bordered on its east by the Gulf Stream. Much of the shoreline consists of barrier islands separated by shifting inlets and backed by riverine estuaries, sounds, lagoons, salt marshes and the Intracoastal Waterway. Riverine input is sporadic. Some areas, like portions of Onslow Bay, are sediment-starved with little riverine input, whereas just to the south is North Carolina's largest and most industrialized riverine system, the Cape Fear River watershed. This river drains directly into the coastal ocean off of North and South Carolina (Mallin et al., 2000). The entire region is subject to

frequent flooding, numerous catastrophic storms and chronic erosion problems. Summaries of a number of previous studies of physical, chemical and biological properties of the continental shelf of the SAB are given by Atkinson et al. (1985).

Due to the social and economic importance of the Carolinas' coastal region, environmental monitoring is increasingly important in the SAB. The University of North Carolina Wilmington has begun an inter-disciplinary, long-term CORMP to understand the physical, biological, chemical and geological aspects of this southern region, as well as impacts of natural and anthropogenic changes on the coastal-ocean resources and their management. One of the objectives within CORMP is the optical characterization of the waters of Onslow Bay,

Table 1
Optical characteristics of two water bodies, Onslow Bay and Cape Fear River Plume, during study period in the South Atlantic Bight, North Carolina, USA[a]

Onslow Bay

Date	a_{CDOM} (350) (m^{-1})	S (nm^{-1})	Chlorophyll a (mg/m^3)	Salinity
20 Nov. 2001	0.13	0.0209	No data	36.5
19 Feb. 2002	0.26	0.0175	0.160	36.6
17 Apr. 2002	0.31	0.0226	No data	35.9
17 June 2002	0.16	0.0162	0.162	36.3
05 Sept. 2002	0.35	0.0228	0.249	35.8
08 Nov. 2002	0.29	0.0176	0.605	36.0
14 Jan. 2003	0.74	0.0176	0.903	35.4
12 Mar. 2003	0.72	0.0165	0.571	35.1
01 May 2003	0.81	0.0194	0.204	34.2
01 July 2003	0.71	0.0107	0.221	35.1
15 Sept. 2003 before Hurricane Isabel	0.30	0.0154	1.071	35.9
23 Sept. 2003 after Hurricane Isabel	0.49	0.0089	0.584	35.6
All data	0.44	0.0206	0.473	35.7

Cape Fear River plume

Date	a_{CDOM} (350) (m^{-1})	S (nm^{-1})	Chlorophyll a (mg/m^3)	Salinity	Cape Fear River discharge ($m^3\,s^{-1}$)
12 Dec. 2001	0.74	0.0198	4.7	36.1	52.3
22 Jan. 2002	2.67	0.0168	3.5	27.2	470.2
24 Apr. 2002	1.21	0.0165	1.6	33.9	137.8
24 June 2002	0.43	0.0177	1.3	35.0	27.9
26 Aug. 2002	0.68	0.0180	2.8	36.5	18.6
18 Sept. 2002	1.31	0.0172	2.4	34.6	74.1
22 Oct. 2002	1.94	0.0168	3.8	34.4	382.2
19 Nov. 2002	2.31	0.0175	1.4	31.7	481.1
30 Jan. 2003	2.19	0.0161	2.4	32.7	110.0
18 Feb. 2003	1.67	0.0167	1.4	33.1	291.6
21 Apr. 2003	7.47	0.0216	2.1	28.6	1063.1
27 May 2003	3.40	0.0156	2.4	30.5	830.6
26 June 2003	9.90	0.0153	3.0	27.3	357.6
12 Aug. 2003	8.42	0.0154	5.1	28.1	1088.2
22 Sept. 2003	2.29	0.0156	2.1	33.7	245.5
All data	3.20	0.0171	2.7	32.2	371.3

Note: The sampling grid in September 2003 was changed. Stations CFP3 and CFP4 (Fig. 1) were omitted. Two additional stations CFP8 and CFP9, located west of the previous sampling grid (not shown on the figure) were sampled.

[a]Average surface water values of CDOM absorption coefficient at $\lambda = 50$ nm, ($a_{CDOM}(350)$), spectral slope coefficient ($S_{300-500}$), chlorophyll a concentration, salinity and Cape Fear River flow.

the Cape Fear River Plume and coastal south-eastern North Carolina. Changes in optical properties of water masses may be used to compare physicochemical processes within, and exchange between, the coastal system of Onslow Bay and the adjacent estuarine system of the Cape Fear River plume. Coastal and estuarine waters differ greatly in their IOP and AOP. Environmental conditions, that determine IOP and AOP of sea water in the study area during field observations, are listed in the Table 1. Average values of CDOM absorption coefficient $a_{CDOM}(350)$, spectral slope coefficient, $S_{300-500}$, chlorophyll *a* (Chl-*a*) concentrations, values of salinity and Cape Fear River flow are given for each cruise in the Onslow Bay and Cape Fear River plume area. In Onslow Bay, clear water, low in particulate matter and phytoplankton pigment concentrations, reflect the optical characteristics of Case 1 waters, and may be found a few km offshore. In areas influenced by riverine inflow, water optical properties are determined by high CDOM and sediment input as well as enhanced phytoplankton growth. These waters may be classified optically as Case 2 waters. The Cape Fear River serves as a point source of water into the eastern SAB and the river end members of the study region are extremely rich in CDOM (Kowalczuk et al, 2003). In situ optical measurements are needed to compare with estimates derived from SeaWiFS imagery to build a database for refining regional bio-optical models. These data may also be used for further improvement of the accuracy of remote sensing algorithms for chlorophyll and regional estimates of phytoplankton production. Reports on optical properties in the SAB are scarce (Nelson and Guarda, 1995) and these experimental data should provide a valuable addition.

3. Results

3.1. Comparison of in-water and above-water spectral remote sensing reflectance measurements

3.1.1. Data

During this study, 145 spectra of reflectance, downwelling irradiance, and diffuse attenuation coefficients were collected using the MicroPro profiling spectroradiometer. We also collected 120 reflectance spectra using the MicroSAS instrument, which match the time and location of measurements taken with the profiling spectroradiometer. Seventeen additional spectra were recorded using the MicroSAS, along a tract of sonar scans in Onslow Bay, during March 14, 2002 (S1 through S17 on Fig. 1). These spectra were used to assess SeaWiFS-scale sub-pixel variability. Reflectance spectra from the MicroPro were not corrected for instrument shelf-shading effects. In the relatively optically clear waters of Onslow Bay we assumed that self-shading was insignificant, due to the small dimensions of the sensors (6 cm diameter × 26 cm long). Self shading may have an effect on radiometric measurements in turbid waters, e.g. in Cape Fear River plume area, influenced by high concentrations of absorbing materials such as CDOM and particulate matter. Deployment of the free-fall profiling instrument in turbid waters is a challenging task requiring a skillful and experienced operator. The instrument descent speed must be carefully adjusted and regulated with the ballast weights to allow the sensor time to adjust the sensitivity gain switch during descent. A reduced descent rate (we used 0.5–0.8 m s^{-1}) is required in order to collect enough data points in the surface layer to calculate the K_d and K_L coefficients needed to calculate spectral reflectance, especially in the blue 412 and 443 nm wavebands. In the presence of highly absorbing water constituents, light is attenuated so quickly, that the signal drops below the instrument's detection limit in the first few meters. Therefore, the instrument must be released in such a way to let the profiling vehicle become vertical and stabilized just below the water surface, so the top meters of the cast fit into the $\pm 5^{\circ}$ tilt-tolerance bracket.

3.1.2. In-water spectral remote sensing reflectance measurements.

The sharp contrast in optical properties of the two study regions and event-scale temporal changes are very evident from reflectance profiles measured in Onslow Bay and in the Cape Fear River plume during the summer of 2002 and the end of the summer of 2003, after the passage of Hurricane Isabel over coastal Carolina (September 17–18, 2003). Data from the MicroPro profiling radiometer are presented here to illustrate seasonal and event-driven variability in AOPs, and to quantitatively compare two contrasting water masses. The discrimination between Cases 1 and 2 water optical signatures was done upon visual inspection of spectra and comparison to a published record of Morel and Prieur (1977) classification. The spectra were also compared to other classification schemes

(IOCCG 2000; Lahet et al., 2001a, b). This selection was later compared to the numerical procedure for discriminating between Cases 1 and 2 spectral signatures proposed by Ouillon and Petrenko (2005) and based on the magnitude of spectral reflectance values and position of the remote sensing reflectance spectrum peak. The initial discrimination between Cases 1 and 2 waters matched the Ouillon and Petrenko (2005) scheme very well.

The spring and summer of 2002 was a period of severe drought in the Cape Fear watershed, which significantly limited riverine discharge into the coastal ocean (27.9–137.8 $m^3 s^{-1}$). As a result, the input of optically active constituents of terrestrial origin, especially CDOM, was reduced (Kowalczuk et al., 2003) (e.g. average values of selected optically active water constituents in Cape Fear River plume during the June 2003 cruise: $a_{CDOM}(350) = 0.43\,m^{-1}$, Chl-$a = 1.3\,mg\,m^{-3}$). Gulf Stream waters were advected very close to shore in Onslow Bay and into the Cape Fear plume region. Both processes had an impact on the IOP and, thus, AOP. Onslow Bay water was very transparent and had a spectral signature typical of waters optically classified as Case 1, with higher reflectance in the blue and weak reflectance in the red portion of the spectrum (Fig. 2). In August and September 2003, high rainfall and the passage of Hurricane Isabel caused increased CFR discharge ranging from approximately 300–1100 $m^3 s^{-1}$. The high load of dissolved organic matter and particles flushed into the area by the heavy rains and resuspended from the bottom by heavy seas impacted the optical properties of waters as far as 36 km offshore (Station OB20) (e.g. average values of selected optically active water constituents in Onslow Bay $a_{CDOM}(350) = 0.30–0.49\,m^{-1}$, Chl-$a = 1.071–0.584\,mg\,m^{-3}$). The downwelling irradiance and upwelling radiance profiles exhibited optical properties more typical of Case 2 waters: low reflectance values in the blue due to strong absorption in this region of the spectrum and a relative shift of the transmission maximum toward longer wavelengths. The approach and passage of Hurricane Isabel created Case 2 waters for a limited time, similar to those shown in Fig. 3. In contrast, the Cape Fear River plume sites typically exhibit a range from Cases 1 to 2 waters depending on the spatial extent and location of the plume. Profiles acquired in the Cape Fear River plume area in June 2002 are shown in Figs. 3 and 4. These two radiometric profiles were measured at CFP7, a station that is under oceanic influence (Fig. 3) and station CFP1 which is located in the river mouth (Fig. 4). Although, river flow in June 2002 was the minimum recorded during the entire period of observations (18.6 $m^3 s^{-1}$), CDOM absorption is still expressed by a significant reduction of blue and green light with depth. During periods when riverine discharge was higher, the rate of decrease of light with depth was much higher than shown in Figs. 3 and 4. For example, during the high flow (and high CDOM) period of the fall 2002–2003 (CFR discharge 291.6–1088.2 $m^3 s^{-1}$), blue light was totally absorbed in first meter of the water column (data not shown).

Calculated $R_{rs}(\lambda)$ from in-water profile measurements at six stations in Onslow Bay and six stations in the Cape Fear River plume are shown in Fig. 5 to illustrate the range in spatial variability within and between regions. The two time periods shown, June 2002 and September 2003, represent extremes in hydrological conditions. Three types of $R_{rs}(\lambda)$ spectra are characteristic of the coastal ocean off North Carolina. One, typical for optical Case 1 waters (blue waters) and marked on Fig. 5 with the blue line, is characterized by a maximum at 490 nm, elevated values in blue light and near zero values in the red. Spectra of this type were usually recorded in Onslow Bay, on the continental shelf, approximately 16 km or more offshore from Masonboro Inlet (Fig. 1 station OB10). The second type of spectra is typical for optical Case 2 waters (brown or yellow water) and is characterized by maximum in 555 nm, low values in blue light due to CDOM absorption and elevated values in the red due to particle scattering. These spectra, marked on Fig. 5 with the reddish-brown lines, were recorded at Masonboro Inlet (Fig. 1, station OBSB) and at the Cape Fear River plume area. The third type of spectra, marked on the figure with the green line, represents intermediate waters, between the two major optical classifications. These spectra were recorded approximately 8–16 km offshore in Onslow Bay and at the most ocean-ward stations of the Cape Fear River plume. In these waters, most of the particles have already sedimented or precipitated out of the water column, but CDOM absorption may still significantly influence the spectral signature. These spectra usually have lower values through the whole spectrum due to weaker scattering and significant decreases in both the blue and red part of the light spectrum. The maximum absorption is located at 490 nm, similar to Case 1 waters, and the appearance of the water is

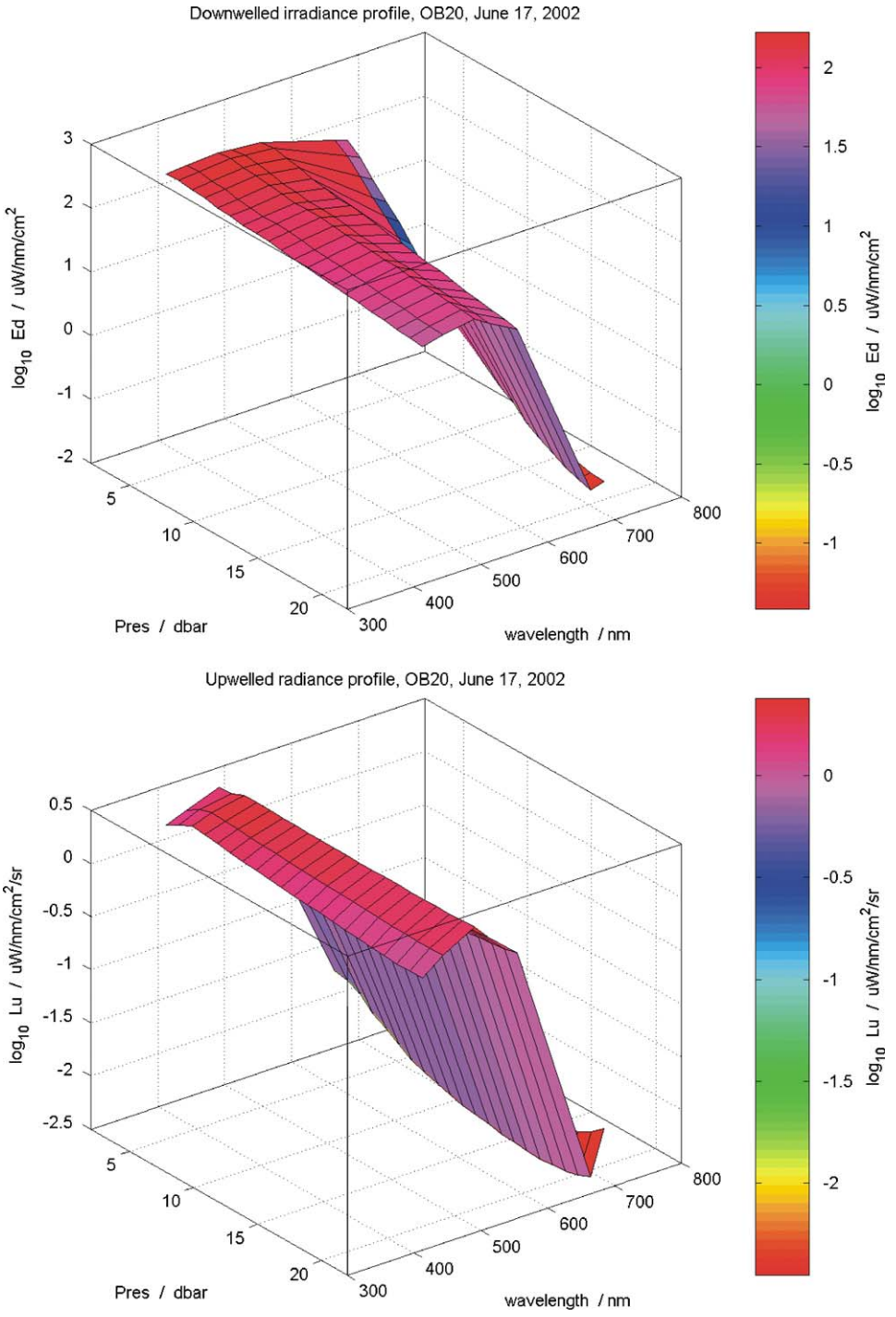

Fig. 2. Example of a downwelling irradiance (top) and upwelling (bottom) radiance profile acquired in optically clean (Case 1) waters in Onslow Bay on Station OB20, on June 17, 2002.

blue-green or green. Those spectra may be classified as blue-green or green, according to classification proposed by Lahet et al. (2001a, b).

There is significant variability in the magnitude of the remote sensing reflectance spectra, caused presumably by differences in particle and CDOM

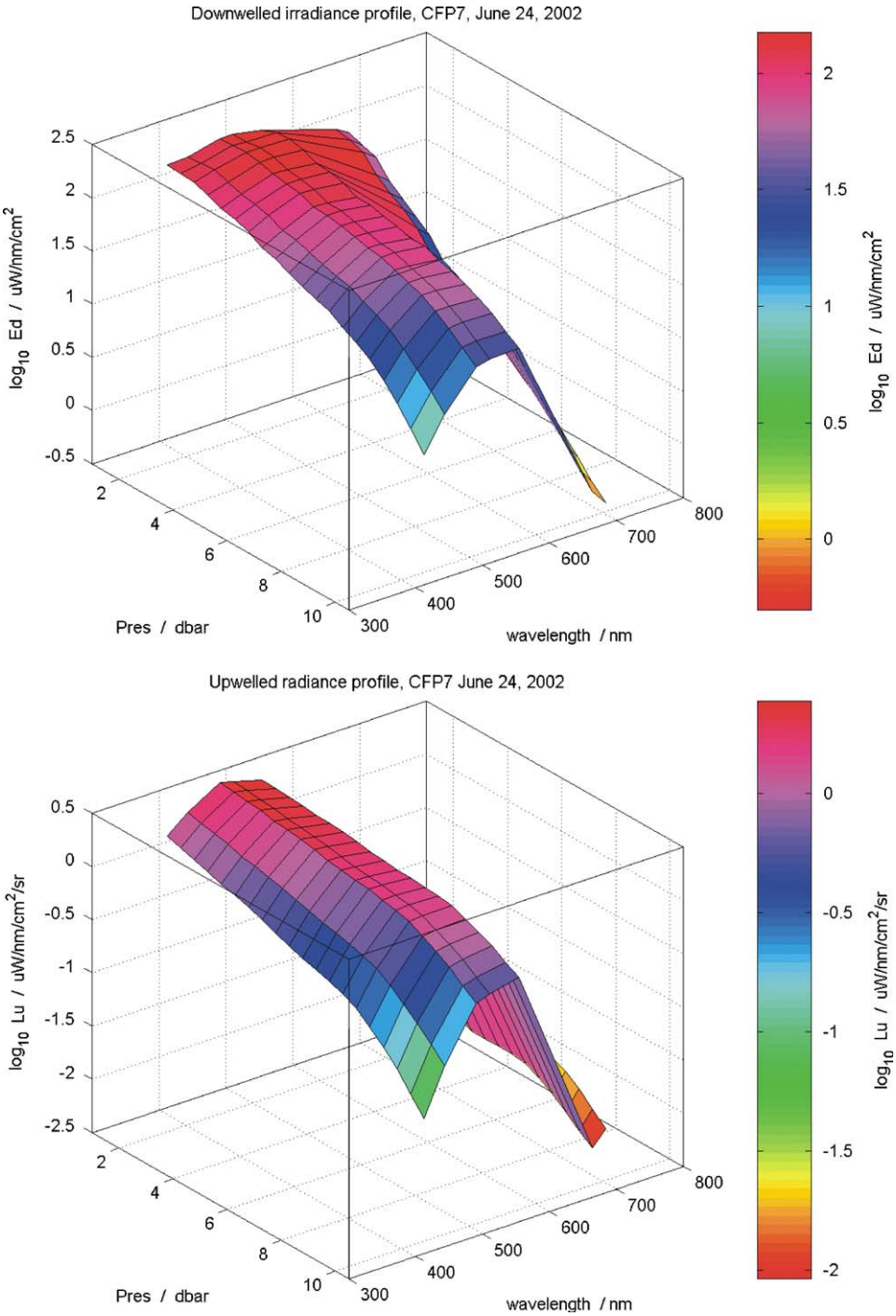

Fig. 3. Example of a downwelling irradiance (top) and upwelling (bottom) radiance profile acquired in optically complex (Case 2) waters of the Cape Fear River plume area on station CFP7, on June 24, 2002, during low flow of Cape Fear River.

concentrations. For example, Onslow Bay remote-sensing reflectance spectra are elevated in September 23, 2003 (Fig. 5c), compared with spectra from the same station during the summer of 2002, June 17 (Fig. 5a). This is likely due to strong backscatter caused by the presence of particles resuspended from the bottom by heavy swell caused by the passage of Hurricane Isabel, five days before the

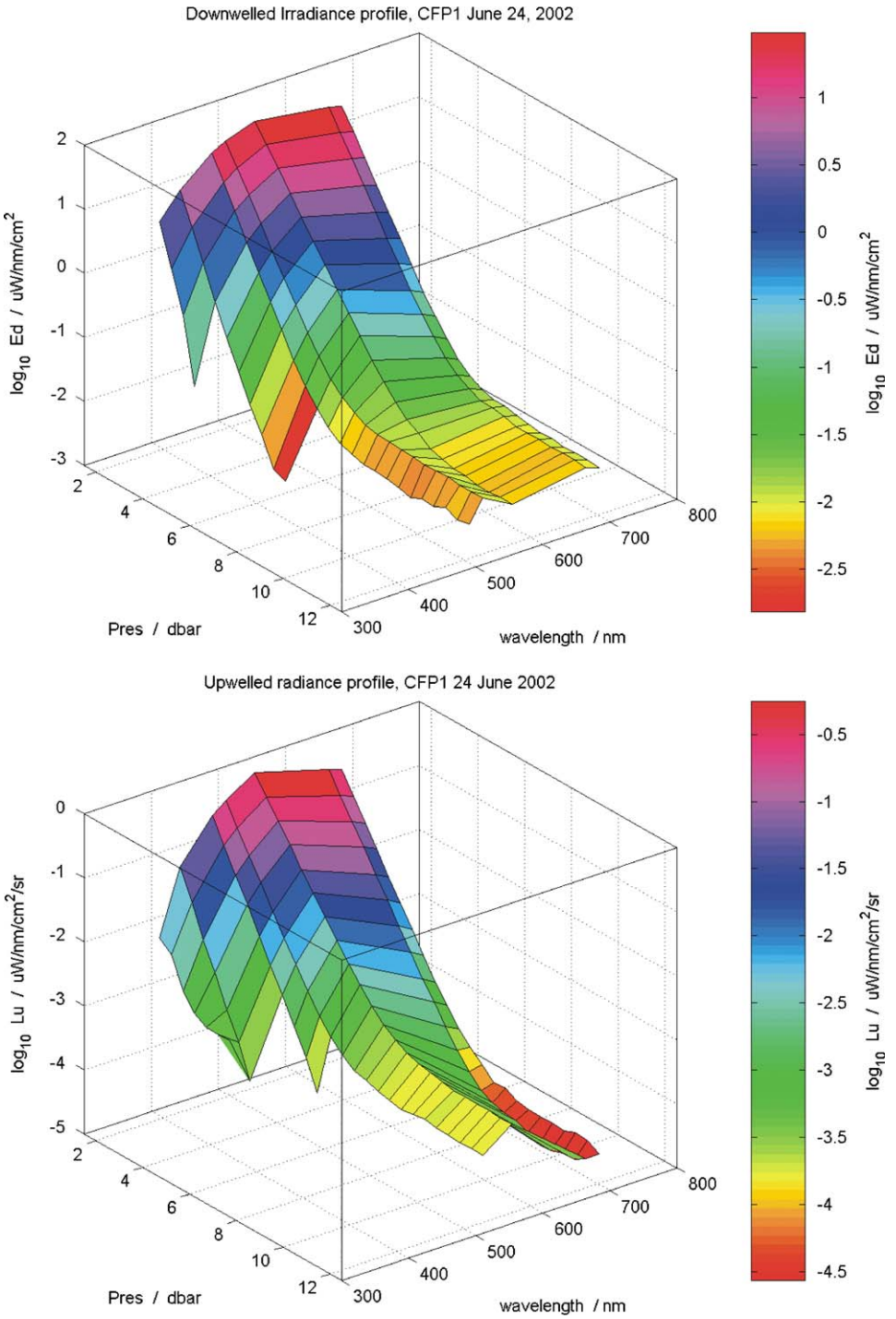

Fig. 4. Example of a downwelling irradiance (top) and upwelling (bottom) radiance profile acquired in optically complex (Case 2) waters of the Cape Fear River plume area on station CFP1, on June 24, 2002, during low flow of Cape Fear River.

spectral measurements had been taken and increased phytoplankton abundance, indicated by elevated chl-*a* concentration (Table 1). In contrast, hurricane-induced changes to reflectance spectra in the plume region appear dominated by the variable effects of CDOM rather than particles. In June 24, 2002, CDOM absorption was relatively low (Kowalczuk et al., 2003) and scattering by particles

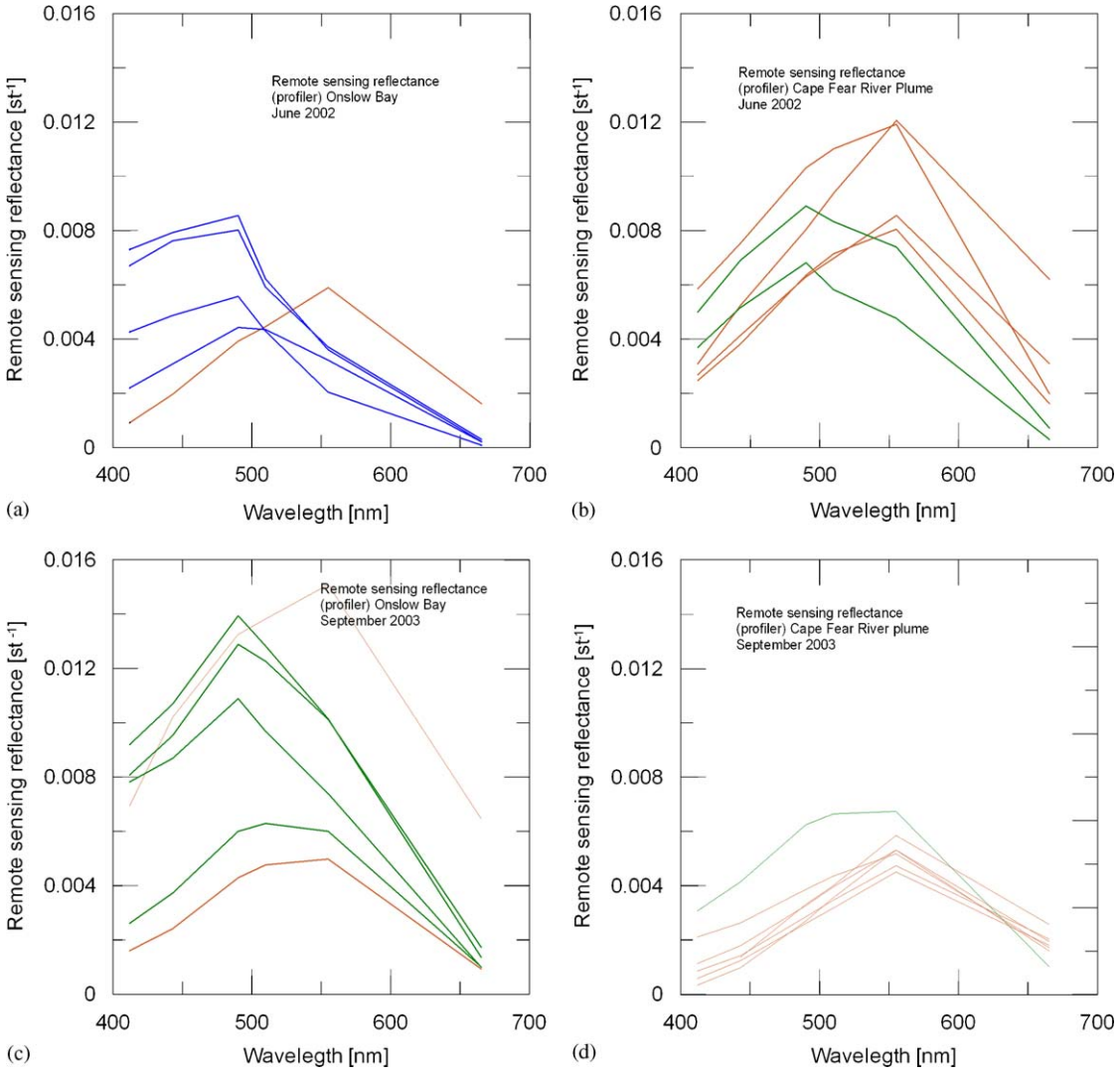

Fig. 5. Examples of remote sensing reflectance spectra acquired in (a) Onslow Bay in June 2002, (b) Onslow Bay in September 2003, (c) the Cape Fear River plume area in June 2002 and (d) the Cape Fear River plume area in September 2003. Blue lines represent Case 1 (blue water) spectra, orange lines denote Case 2 yellow and brown plume-impacted waters, and green lines indicate intermediate Case 2 waters.

(which tends to shift reflectance spectra upwards) led to relatively high reflectances (Fig. 5c). One year later (September 21, 2003) during high flow caused by heavy rainfall from the hurricane, $R_{rs}(\lambda)$ values were lower, due to suppression of upwelling radiance by CDOM-dominated absorption.

3.1.3. Comparison of above- versus in-water spectral reflectance measurement methods

Reflectance spectra measured with the MicroSAS above-water instrument are not shown, because there are only five of seven matching wavebands: 412, 443, 490, 555 and 685 nm. For the comparative study of spectral reflectance measurements obtained with the two methods we used only the first four wavebands. Data were divided into all data (163 samples) and clear-sky data (93 samples). Data were also analyzed according to the location of measurements. All measurements performed in the Cape Fear River plume area and inshore stations at Onslow Bay, OBSB and OB05, were classified as Case 2 waters. The remaining Onslow Bay stations had, for the most part, AOP characteristics of Case 1 waters. We assumed that, none of the

spectral reflectance data set measured in- and above-water should be considered a "true" one. Therefore, the unbiased percent difference (UPD) (Hooker et al., 2002) between the two data products X^A and X^B were calculated as:

$$\psi_B^A(\lambda) = \frac{200}{M}\sum_{i=1}^{M}\frac{\left|X_i^A(\lambda) - X_i^B(\lambda)\right|}{X_i^A(\lambda) + X_i^B(\lambda)}, \quad (3)$$

where, M is the number of measurements and A and B codes identify the method used. In our case A would be related to in-water measurements and B would be related to above-water measurements.

Spectral average of the UPD was calculated by including the summation in Eq. (3) over the four spectral bands: 412, 443, 490 and 555 nm:

$$\bar{\psi}_B^A = \frac{1}{4}\sum_{j=1}^{4}\psi_B^A(\lambda j). \quad (4)$$

Results of comparisons between the two remote sensing reflectance measurement methods are summarized in Table 2. Fig. 6 compares clear sky measurements in- and above-water of remote sensing reflectances at four wavelengths (412, 443, 490, and 555 nm). The ±5% difference threshold from a 1:1 line is marked with dashed lines. Although the data fell along the 1:1 line, substantial scatter exists. Agreement between the MicroPro and MicroSAS data in clear sky is much better, than in comparison to specific spectral reflectance values calculated for all data available (Table 2), with many data points falling within the ±5% accuracy threshold, especially in Case 1 waters. There were more departures from ±5% accuracy threshold in Case 2 waters. Although the illumination conditions were favorable for above-water reflectance measurements, there are some noticeable outliers in the data that significantly impacted accuracy. Possible sources of errors in above-water measurements may be associated with ship movements, foam generation by the ship's hull and propeller wash.

Agreement between in-water and above-water $R_{rs}(\lambda)$ measurements was best for the 490 nm waveband, Case 1 waters, and cloud-free conditions. The lowest difference was recorded for the 490 nm waveband and the largest difference was for the 555 nm waveband (in all four data subsets analyzed). The spectrally averaged UPD calculated for the following four data subsets was: (1) all measurements—42.4%; (2) measurements in cloud free conditions—39.8%; (3) cloud free conditions in Case 2 waters—47.3%; (4) cloud free conditions in Case 1 waters—26.7% (Table 2). Protocols for in- and above-water measurements may need to be revised, especially for turbid plume waters to achieve the ±5% difference threshold from the 1:1 line. The deviations appear to be due to noise rather than systematic differences (as evidenced by the nearly 1:1 correspondence in data sets), which suggests that the data could be examined

Table 2
Statistics of calculated unbiased percent differences (UPD) between in-water and above-water spectral remote sensing measurements

Data set	Wavelength	Max. difference %	Min. difference %	Mean difference %	Std. Dev. %	Sample size M
All data	412	97.6	0.1	49.4	23.5	163
	443	99.9	0.1	39.3	20.2	
	490	79.9	0.1	30.2	15.6	
	555	157.0	0.1	50.6	25.1	
Clear sky, all data	412	95.4	0.3	49.7	24.3	93
	443	99.9	0.1	38.9	21.9	
	490	79.9	0.1	26.9	15.8	
	555	99.6	0.2	43.6	21.2	
Clear sky, Case 2 waters	412	95.4	0.2	64.1	28.2	64
	443	99.9	0.1	48.8	24.3	
	490	79.9	0.1	32.5	17.4	
	555	99.6	0.1	43.8	23.6	
Clear sky, Case 1 waters	412	67.2	0.5	29.1	16.3	29
	443	51.4	0.3	19.5	12.1	
	490	37.1	0.2	14.3	9.1	
	555	66.1	0.5	43.8	13.9	

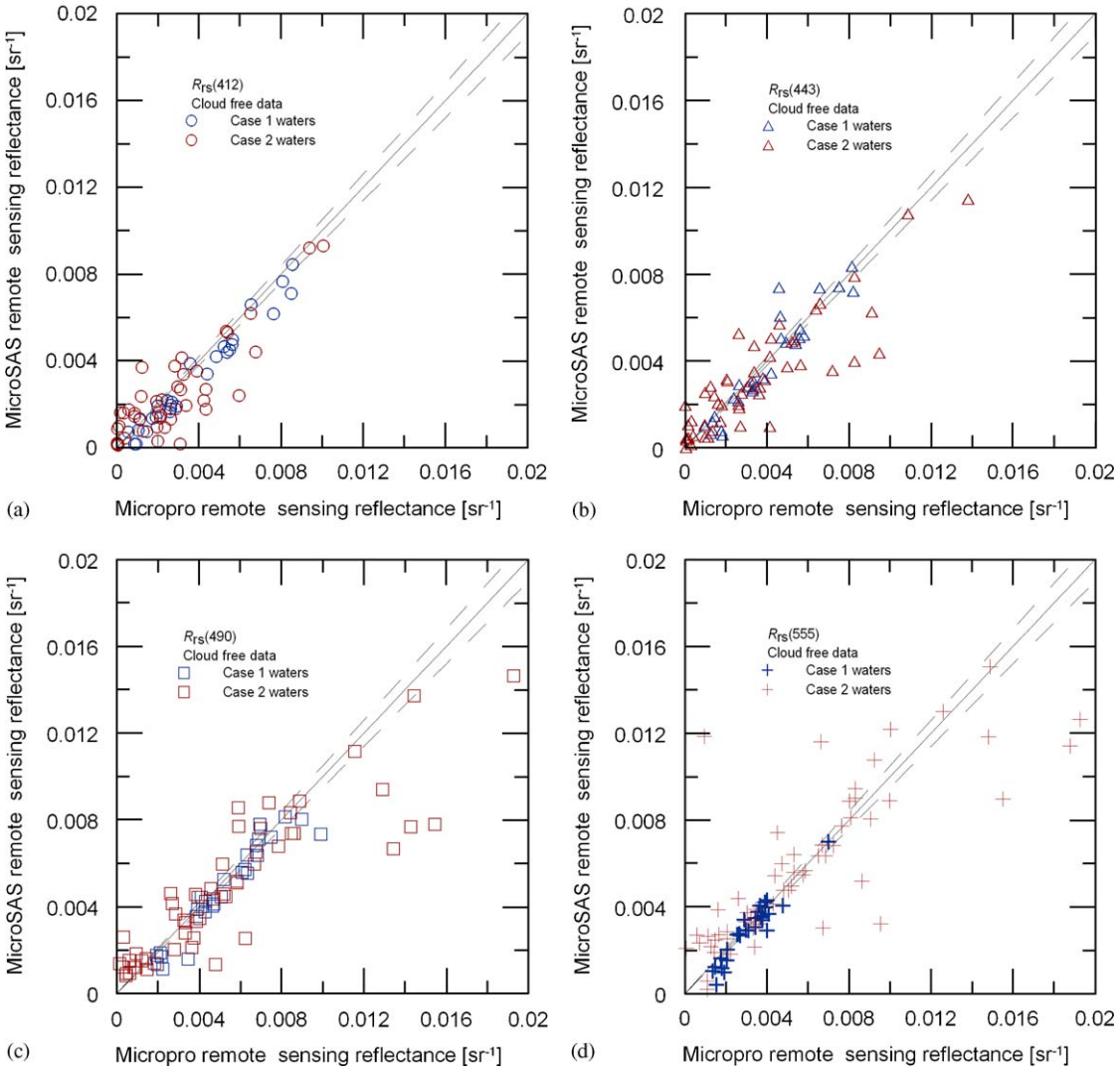

Fig. 6. Comparison of cloud free remote sensing reflectance data measured in-water (Micropro profiler) and above water (MicroSAS radiometer) in the South Atlantic Bight. The dashed line represents the $\pm 5\%$ accuracy threshold.

statistically to determine factors contributing to this noise, possibly enabling the refinement of sampling protocols so that inimical sampling conditions could be avoided during future monitoring efforts.

3.2. Comparison of measured radiometric quantities with SeaWiFS data estimates

We used four SeaWiFS scenes to compare the radiometric quantities measured in situ (data from Satlantic profiling Micropro radiometer were used as sea-truth data) with respective estimates derived from satellite imagery on 24 October 2001, 22 January 2002, 17 April 2002 and 24 June 2002. SeaWiFS scenes were processed using SEADAS 4.1 processing software and the default atmospheric correction protocol. For those four days we have 24 matching point measurements of remote sensing reflectance, and downwelling-irradiance diffuse-attenuation coefficient. The maximum time difference between the in situ measurements and the satellite overpass was 3 h 40 min after the SeaWiFS data scan. All SeaWiFS data for the study area were flagged for shallow water, and thus the remote sensing reflectance signal may be influenced by bottom reflection. Our ground-truth measurements were also not corrected for bottom reflection.

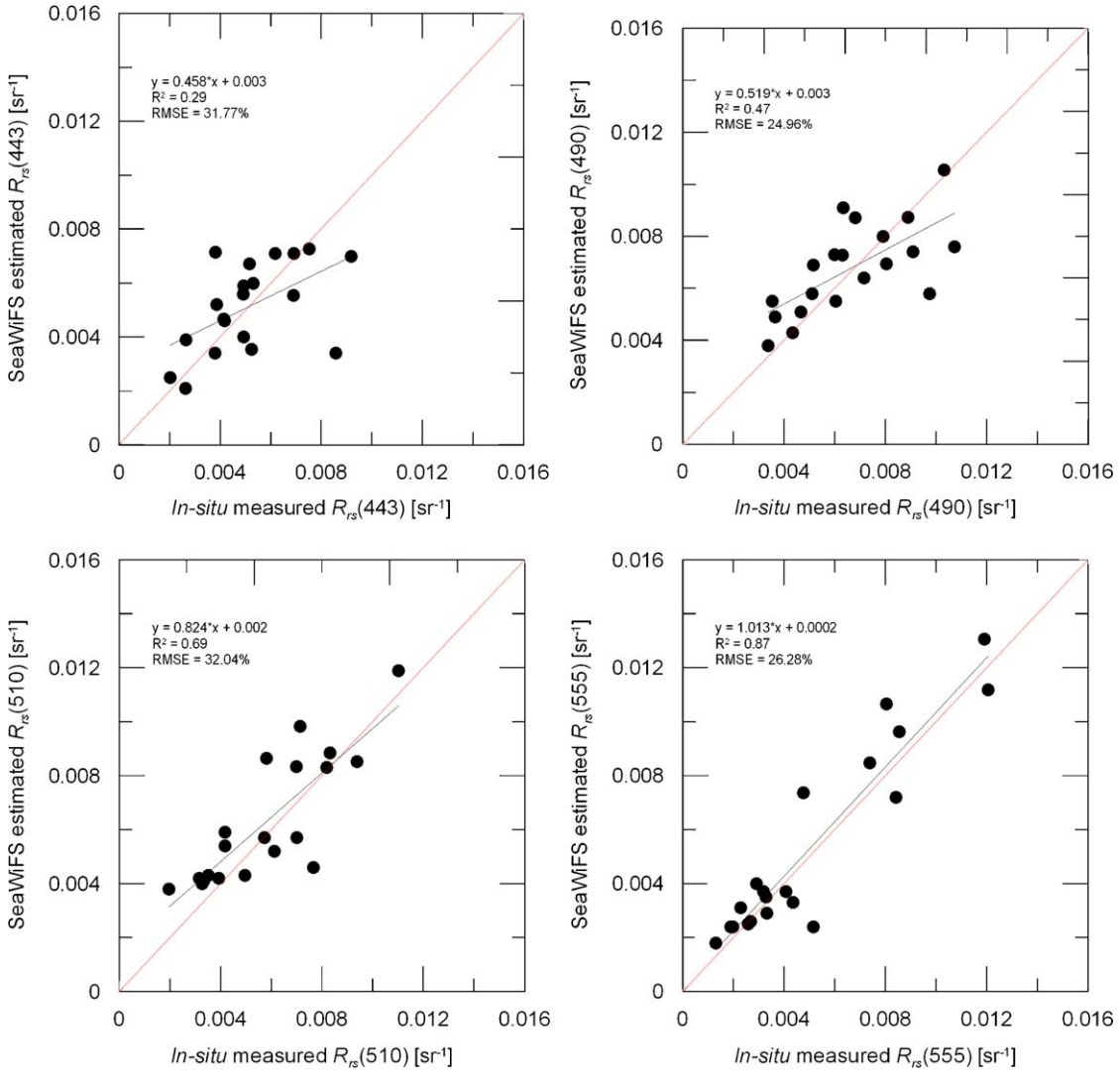

Fig. 7. Comparison between remote sensing reflectance measured in situ and estimated from SeaWiFS imagery data.

Comparisons between measured and SeaWiFS estimated values of remote sensing reflectance (Fig. 7) indicated the lowest agreement for the 412 nm waveband. The ground-truth data and satellite estimates were not correlated and the random mean square-root error (RMSE) of the estimate was 56.78%. This lack of correspondence may be the result of a failure in the atmospheric correction algorithm, as suggested by cloud-free pixels with negative $R_{rs}(4\,1\,2)$ values in our data set. Comparability between in situ measurements and satellite estimates was greatly improved for longer wavelengths, which showed lower root mean square errors (RMSE) of: 31.77% at 443 nm, 24.96% at 490 nm 32.04% at 510 nm, and 26.28% at 555 nm. Although the smallest RMSE was calculated for the 490 waveband, the correlation between in situ measurements and satellite estimates was low ($R^2 = 0.47$). For the 555 waveband we obtained the best-fit equation ($R^2 = 0.87$), and the second-lowest RMSE; hence the in situ/satellite agreement is deemed best at 555 nm.

Comparisons between measured values and SeaWiFS estimates of diffuse attenuation coefficient for $\lambda = 490$ nm exhibited a reasonable agreement, with a calculated RMSE of 34.31%. Although in situ and estimated values of K_d (490) are correlated ($R^2 = 0.75$), the SeaWiFS standard algorithm tends to severely underestimate the K_d (490) in the coastal zone of North Carolina (data not shown).

The maximum difference in our data set was observed for Station CFP2, near the Cape Fear River mouth. The measured K_d (490) value was underestimated over 3 times by the corresponding SeaWiFS estimate. This result is not surprising, considering that: (1) the 412 nm SeaWiFS data were often negative and (2) there is a high prevalence of CDOM in the region which is not correlated with phytoplankton sources, unlike the data set used to derive the K490 algorithm (O'Reilly et al., 1998). Future work with this data set will focus on the determination of local algorithms. In the clear water of the continental shelf, discrepancies were much smaller, and the error of estimation could result both from algorithm inaccuracy and in situ measurement error due to difficulties in getting data near the sea surface. In most cases the measurements were taken in clear, optically Case 1 waters. On the shallow continental shelf, where mean depth is approximately 30 m, it was impossible to get a light profile which fulfilled the SeaWiFS Ocean Optics Protocol recommendation (the full profile should contain at least three optical depths). Light profiles taken in Onslow Bay are usually less than two optical depths.

3.3. Sub-pixel variability estimation

To assess the effects of sub-pixel variability on the above satellite matchups in the region, we ran one experiment on 14 March 2002, within a small polygon in Onslow Bay (Fig. 1). The ship cruise track was dictated by towed sonar operations which limited spatial coverage to a region 5×5 km, encompassing little variety in optical properties. We used the MicroSAS instrument configured to take automatic measurements every 10 min along the ship track. The ship cruised along an undulating track, which ran from NW to SE in direction. Each track was separated by approximately 1 km. Optical measurements were taken every second track, when the ship was moving SE, so the instruments were looking on the sun illuminated sea surface, away from the ship shadow. Instrument azimuth angle was continuously adjusted to be 90–120° away from the sun azimuth angle. The ship was cruising at a speed of approximately 6 knots, so each measurement was at least 2 km apart. We took one measurement at the beginning, in the middle and at the end of each track. Altogether we collected 17 spectral measurements, which covered an area of 7 SeaWiFS pixels. Measurements were conducted during the outgoing tide in calm seas, with swells less than 0.6 m, and wind-wave heights of 0.3 m. Sky conditions were overcast during the first 2 h of the experiment, followed by clear sky conditions for the rest of the experiment. The SeaWiFS scene was cloud free over the experiment site.

For the seven pixels covered by the measuring polygon, four have at least three ground-truth spectral measurements (pixels 1, 2, 4, and 6). The SeaWiFS estimates and in situ measured spectral values of remote sensing reflectance for those pixels are plotted on Fig. 8. The ground-truth data seem to be much less variable than the discrepancies between in situ measurements and imagery data estimates. The biggest difference can be seen at the 412 and 555 wavebands. $R_{rs}(412)$ is underestimated by SeaWiFS, possibly due to overcorrection for atmospheric effects, as noted by many researchers (e.g., Sturm and Zibordi, 2002; Bulgarelli and Zibordi, 2003). The in situ measurements at Pixel 2 show more scatter, and correspond to a change of illumination conditions from overcast to clear sky conditions during sampling at that location. When the measurement conditions were stable, scatter in the ground truth data is significantly smaller, except for the 555 waveband (Fig. 8, Pixels 4 and 6). Remote sensing reflectance values in this waveband is determined to a great extent by scattering of suspended particles; because this waveband is outside of the maximum absorption by phytoplankton pigments and CDOM absorption in this spectral region is very small. In the coastal zone, concentrations of suspended particles are highly variable, and this is a source of variation in the $R_{rs}(555)$ values.

To quantify the dispersion in the ground-truth and satellite data sets we calculated descriptive statistics: mean, standard variation and median for the four matching wavebands (Table 3). The SeaWiFS OC4 standard algorithm, implemented in SEADAS v4.1, tends to underestimate the $R_{rs}(412)$, and we found the highest dispersion in our data set in that waveband (the standard deviation is more than twice that of the in situ data). A high data dispersion of the satellite estimates also occurred in the 443 nm waveband. For the other two wavebands, we calculated similar standard deviations and estimates are within the error threshold calculated for the available Onslow Bay ground-truth data. We conclude that sub-pixel variability was a minor source of discrepancies between

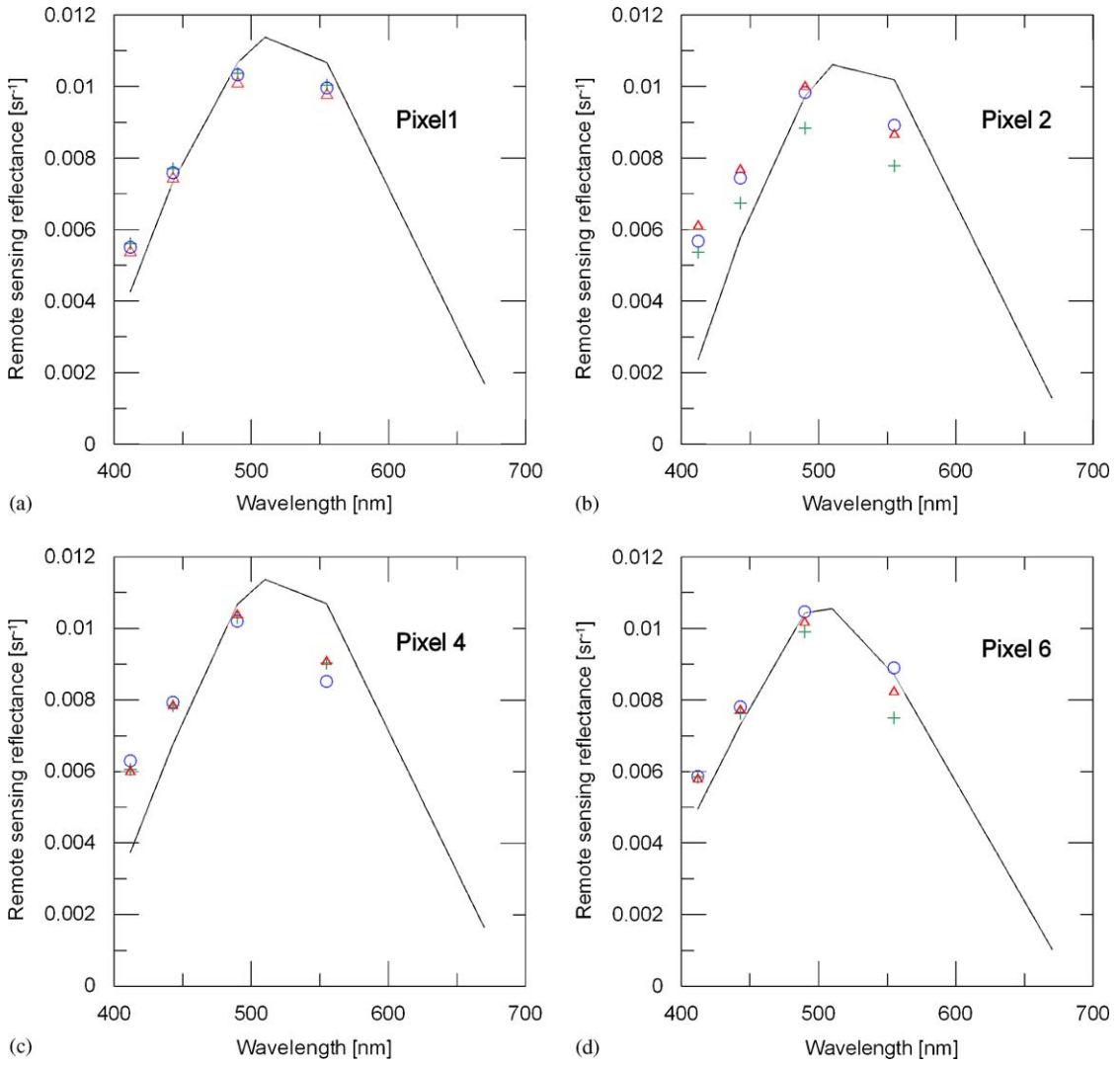

Fig. 8. Examples of SeaWiFS estimated remote sensing reflectance spectra (solid lines) and in situ measured remote sensing reflectance (crosses, triangles and circles) for selected pixels of the sub-pixel variability experiment.

Table 3
Descriptive statistical parameters calculated for in situ measured and SeaWiFS estimated spectral reflectance during sub-pixel variability assessment experiment

	In situ measured $R_{rs}(\lambda)$, $n = 17$				SeaWiFS estimated $R_{rs}(\lambda)$, $n = 7$			
	R_{rs} (412)	R_{rs} (443)	R_{rs} (490)	R_{rs} (555)	R_{rs} (412)	R_{rs} (443)	R_{rs} (490)	R_{rs} (555)
Mean	0.0057	0.0075	0.0100	0.0087	0.0040	0.0069	0.0104	0.0096
SD	0.0004	0.0004	0.0005	0.0008	0.0009	0.0006	0.0004	0.0008
Median	0.0058	0.0077	0.0101	0.0086	0.0042	0.0073	0.0106	0.0092

ground-truth data and satellite estimates in the study polygon, although larger-scale experiments would be necessary to make the same conclusion for all of Onslow Bay.

4. Discussion and conclusions

The coastal ocean in the SAB is a very dynamic environment. IOP and AOP in this region are

controlled to a great extent by superposition of complex systems of oceanic and atmospheric cycles, which control border conditions (e.g. Gulf Stream meanders) and precipitation on the coastal plain. At small spatial and temporal scales, there is a significant influence of terrestrial material from the coastal plain transported to the ocean. Durako et al. (2002) and Kowalczuk et al. (2003) have shown the high degree of variability of IOPs that exists in the Cape Fear River plume area and Onslow Bay. These optical changes are directly linked with variation in river flow, the quantity and nature of transported material and differences in the relative contributions of dissolved and particulate material. This unique external condition creates an environment where, in the distance of tens of kilometers, both the most optically complex and clearest natural waters may be found. Frequent catastrophic events, like hurricanes, add even more disturbances to this already dynamic region. Impacts of hurricanes on the optical properties of water have been documented by Sosik et al. (2001) and Boss et al. (2001) on New England shelf waters during the Coastal Mixing and Optics experiment in August 1996. High seas caused by hurricane-force winds broke the summer stratification and resulted in resuspension of particles from the bottom (depth ~70 m) and the release of CDOM accumulated in bottom sediments, as shown by increases in the level of particulate and CDOM absorption and increased magnitude of the particle-backscattering coefficient recorded in vertical profiles of those parameters. They also showed that an increased concentration of particles has the most significant impact on spectral reflectance. Station OB20, located 36 km southeast of Masonboro Inlet, is only 23 m deep, so similar processes were certainly responsible for increased particle loads leading to elevated values of $R_{rs}(\lambda)$. Wren and Leonard (2005) have published a record of significant resuspension of bottom sediment and sediment deposits replacement caused by Hurricane Isabel in Onslow Bay. Changes in the reflectance spectrum in the blue, following the passage of Hurricane Isabel, presumably resulted from increased CDOM absorption, which could have been flushed from the bottom or originated in terrestrial runoff.

Observed changes in spectral signatures of water are frequently reported in areas which are under the influence of riverine outflow. Shifts of the reflectance maxima toward longer wavelengths, caused mainly by increased CDOM absorption have been reported by Kowalczuk et al. (2005) in the Baltic Sea, Darecki et al. (2003); in the shelf waters west off Ireland, D'Sa and Miller (2003); in the Gulf of Mexico at the vicinity of Mississippi River outlet; Froidefond et al. (2002) along French Guiana coast under the influence of Amazon River, and most recently by Harding et al. (2005) for the Chesapeake Bay. Lahet et al. (2001b) also reported changes in color from yellowish-greenish to blue in the transition from the Ebro estuary to the oligotrophic waters of the eastern Mediterranean. Changes in the spectral signatures of water may be applied to the classification of water based on color, which may improve remote sensing algorithms for the retrieval of bio-optical parameters. This approach was applied in the Baltic Sea by Darecki et al. (1995), by Lahet et al. (2001a) in the eastern Mediterranean, and by Moore et al. (2000) for the global classification of water based on color.

Frequent changes in IOP and AOP of water in the SAB requires frequent and regular sampling to build a large data set of in situ measurements for testing of existing remote sensing algorithms, retrieval of bio-optical parameters, and their optimization to local conditions. Use of above-water radiometers enables much better spatial resolution of spectral remote sensing measurements. The radiometric data base, collected during the CORMP program from October 2001 to September 2003 and presented in this paper, enabled us to compare the use of above-water to in-water measurements of $R_{rs}(\lambda)$ for routine operational oceanography in the study area. Our results are more variable than those reported by Hooker et al. (2002) and Zibordi et al. (2002), but our instruments were placed on a moving small vessel instead of a fixed platform. The calculated differences between in-water and above-water measurements in the range of 40% for the entire data set we consider unsatisfactory. However, when there were favorable conditions for above-water measurements, like those modeled by Mobley (1999)—clear sky and calm sea we achieved better agreement between the two methods. In the 443 and 490 wavebands the unbiased percent difference calculated for data collected during favorable conditions were, at 15–20%, still above the $\pm 5\%$ accuracy threshold, and the 412 and 555 wavebands greatly exceeded this limit. A report by Hooker et al., 2004 showed that, good accuracies between in-water and above-water spectral radiance measurements can be obtained from a small boat in relatively turbid coastal water, when

above-water radiometers were stabilized by a cardanic gimbal and data were corrected for bidirectional effect of reflection and refraction (so-called Q-function). The general conclusion that needs to be emphasized is, that above-water radiometric measurements very much depended on illumination conditions and may performed only on calm seas for clear or overcast skies, when sky radiance has uniform radiance distribution and only those data should be used for algorithm development. In practice, for routine monitoring cruises those conditions are rarely satisfied, so use of both in-water and above-water methods should be recommended. Limitations of in-water radiometric measurements in optically complex waters and at shallow depths may be overcome by using modified instrumental setup and correction factors, as recommended by the measurement protocol.

Ship-based sampling is a necessity in most coastal regions where fixed oceanographic platforms do not exist, and it provides the opportunity to sample waters of varying optical properties, rather than being limited to the optical environment of a single site. However, shipboard measurements present a much more complex measuring environment than exist on fixed platforms, increasing measurement noise due to the ship's pitch and roll motion, foam generation by waves reflected by the ship's hull, etc., and restricting the choice of weather conditions and viewing geometry. These factors are expected to contribute to higher differences between measurement methods. However, examples of novel approaches for above-water radiance measurements and algorithms for sun-glint removal, suggest that above-water radiance measurements from ships is a very promising tool (e.g. Olszewski and Kowalczuk, 2000; Wood and Cunnigham, 2001). New field data and sampling protocols should help to reduce the discrepancies between in-water and above-water radiance measurements, enabling the use of various radiometric data sets for monitoring optical properties of water masses in the complex coastal environment. The potential of the MicroSAS instrument for increasing spatial resolution has been shown in the example of our sub-pixel variability experiment. However, use of a more stabilized radiometer platform would help to eliminate errors associated with ship movements. For example, the use of a gyroscope-stabilized platform for placing radiometers on a ship has reduced the platform instability to only $\pm 2^{\circ}$ both in horizontal and vertical axes (J. Olszewski, *personal communication*).

River-impacted coastal margins are highly dynamic regions where the use of global-ocean color algorithms may not be appropriate for accurate estimation of bio-optical variables. We have demonstrated that SeaWiFS estimates of spectral values of remote-sensing reflectance agree within 30–50% of in situ measurements. This range of accuracy from the SeaWiFS standard product is consistent with the results of an evaluation study by Gregg and Casey (2004). They found that overall SeaWiFS global chl-*a* product accuracy is 31%. The regional comparison for SeaWiFS chlorophyll *a* products for the Eastern US Atlantic coast gave an accuracy of 38%. Although they did a global and regional match of analysis for chlorophyll *a* concentration products, we may assume that in our case similar results would be obtained, because the O'Reilly et al. (2000) OC4v4 chl-*a* concentration retrieval algorithm was based on blue:green band ratio. Our assumption was based on results of a comparison of radiometric quantities measured in situ and estimated from SeaWiFS observations done in the Baltic Sea by Darecki and Stramski (2004). They found that direct comparison, of spectral values of normalized water-leaving radiance, was very poor, but the band ratios were much better. Therefore the comparison of chlorophyll *a* estimates from SeaWiFS OC4v4 algorithm in the SAB should fit into the regional accuracy assessment by Gregg and Casey (2004). The riverine plume influences the accuracy of estimated radiometric quantities from satellite observations in the coastal ocean, as shown by Froidefond et al. (2002). Their comparison of in situ and SeaWiFS data along the French Guiana coast influenced by the Amazon River plume gave an accuracy of 68%. Better comparative results were achieved for blue-green light than for blue wave bands, also consistent with the Gregg and Casey (2004) conclusions and Harding et al. (2005). Direct comparison of other SeaWiFS products—K_d (490) (RMSE = 34.1%, $R^2 = 0.75$) may be considered quite good, although the SeaWiFS K490 algorithm tends to underestimate the K_d (490) in the Cape Fear River Plume. Improvements to the agreement between satellite estimates and in situ data were observed for data collected farther offshore in optically clearer waters [as presented for K_d (490)], similar to the recent observations of Harding et al. (2005) in the mid-Atlantic bight offshore of Chesapeake Bay. Darecki and Stramski (2004) have estimated an accuracy of retrieval of that coefficient from MODIS data in the

Baltic Sea of 162%. Satellite observations of K_d (490) may be potentially used for calculations of CDOM absorption in the coastal ocean. Del Vecchio and Subramaniam (2004) found a significant correlation between K_d (490) and a_{CDOM} (490) in the western tropical North Atlantic Ocean. The acquisition of a larger data set of bio-optical variables in coastal Carolina over a longer period of time will allow for refinement of remote sensing algorithms, and is particularly needed for atmospheric and bottom-reflectance corrections in coastal systems, and for the estimation of chlorophyll *a* content and CDOM absorption from ocean color satellite data.

Acknowledgments

This study was supported by NOAA (Grant No. NA16RP2675) through the Coastal Ocean Research and Monitoring Program, Center for Marine Science, University of North Carolina Wilmington, and by Statutory Research Programme no. II.5, at the Institute of Oceanology, Polish Academy of Sciences, Sopot, Poland. Authors would like to thank Dr Giuseppe Zibordi from Joint Research Centre, Ispra, Italy for valuable comments and discussion on the manuscript. Authors would also like to thank J. Brooke Landry, UNCW, for graphical design of Fig. 1. Finally, we would like to thank two anonymous reviewers for their comments on the manuscript.

References

Atkinson, L.P., Menzel, D.W., Bush, K.A. (Eds.), 1985. Oceanography of the Southeastern US Continental Shelf, Coastal Estuarine Science Series 5. AGU Washington DC.

Boss, E., Pegau, W.S., Zaneveld, J.R., Barnard, A.H., 2001. Spatial and temporal variability of absorption by dissolved material at a continental shelf. Journal of Geophysical Research 106, 9499–9507.

Bulgarelli, B., Zibordi, G., 2003. Remote sensing of ocean colour: accuracy assessment of an approximate atmospheric correction method. International Journal Remote Sensing 24, 491–509.

Darecki, M., Olszewski, J., Kowalczuk, P., 1995. A preliminary study of the spectral characteristics of the upward radiance field in the surface layer of the Baltic. An empirical algorithm for remote detection of chlorophyll concentration. Studia i Materiały Oceanologiczne 68, 27–49.

Darecki, M., Weeks, A., Sagan, S., Kowalczuk, P., Kaczmarek, S., 2003. Optical characteristics of two contrasting Case 2 waters and their influence on remote sensing algorithms. Continental Shelf Research 23, 237–250.

Darecki, M., Stramski, D., 2004. An evaluation of MODIS and SeaWiFS bio-optical algorithms in the Baltic Sea. Remote Sensing of Environment 89, 326–350.

Del Vecchio, R., Subramaniam, A., 2004. Influence of the Amazon River on the surface optical properties of the western tropical Atlantic Ocean. Journal of Geophysical Research 109.

D'Sa, E.J., Miller, R.M., 2003. Bio-optical properties of in waters influenced by the Mississippi River during low flow conditions. Remote Sensing Environment 84, 538–549.

Durako, M.J., Kowalczuk, P., Souza, J.J., Mallin, M.A., McIver, M.R., 2002. Spatial and temporal variation in CDOM in a coastal blackwater river plume. In: Steven G. Ackleson (Ed.), Proceedings of Ocean Optics XVI Conference, paper no. 18, 10pp., Santa Fe, New Mexico, USA, 18–22 November 2002.

Fargion, G.S., Mueller, J.L. (Eds.), Ocean optics protocols for satellite ocean color sensor validation, Revision 2. NASA/TM-2000-209966, NASA Goddard Space Flight Center, Greenbelt, Maryland, 184pp.

Froidefond, J.M., Gardel, L., Guiral, D., Parra, M., Ternon, J.F., 2002. Spectral remote sensing reflectances of coastal waters in French Guiana under the Amazon influence. Remote Sensing of Environment 80, 225–232.

Froidefond, J.M., Ouillon, S., 2005. Introducing a mini-catamaran to perform reflectance measurements above and below the water surface. Optics Express 13, 926–936.

Garver, S.A., Siegel, D.A., 1997. Inherent optical property inversion of ocean color spectra and its biogeochemical interpretation: 1. Time series from Sargasso Sea. Journal Geophysical Research 102, 18607–18625.

Gordon, H.R., 1989. Dependence of the diffuse reflectance of natural waters on the sun angle. Limnology and Oceanography 34, 1484–1489.

Gordon, H.R., Clark, D.K., Brown, J.W., Brown, O.B., Evans, R.H., Brinks, W.W., 1983. Phytoplankton pigment concentration in the Middle Atlantic Bight; Comparison of ship determination and CZCS estimates. Applied Optics 22, 20–35.

Gregg, W.W., Casey, N.W., 2004. Global and regional evaluation of the SeaWiFS chlorophyll data set. Remote Sensing of Environment 93, 463–479.

Harding, L.W., Magnuson, A., Mallonese, M.E., 2005. SeaWiFS retrievals of chlorophyll in Chesapeake Bay and the mid-Atlantic bight. Estuarine, Coastal and Shelf Science 62, 75–94.

Hooker, S.B., Zibordi, G., Lazin, G., McLean, S., 1999. The SeaBOARR-98 Field Campaign. NASA Technical Memorandum 1999-206892, Volume 3; SeaWiFS Postlaunch Technical Report Series, In: Hooker, S.B., Firestone, E.R. (Eds.), 40pp.

Hooker, S.B., Lazin, G., Zibordi, G., McLean, S., 2002. An evaluation of above- an in-water methods for determining water leaving radiances. Journal of Atmospheric and Ocean Technology 19, 486–515.

Hooker, S.B., Zibordi, G., Berthon, J.-F., Brown, J.W., 2004. Above-water radiometry in shallow coastal waters. Applied Optics 43, 4254–4268.

IOCCG, 2000. Remote sensing of ocean colour in coastal and other optically complex waters. In: Sathyendranath, S. (Ed.), Reports of the International Ocean Colour Coordinating Group, No. 3. IOCCG, Dartmouth, Canada, p. 145.

Kirk, J.T.O., 1984. Dependence of relationship between inherent and apparent optical properties of water on solar altitude. Limnology and Oceanography 29, 350–356.

Kowalczuk, P., Cooper, W.J., Whitehead, R.F., Durako, M.J., Sheldon, W., 2003. Characterization of CDOM in organic rich river and surrounding coastal ocean in the South Atlantic Bight. Aquatic Sciences 65, 381–398.

Kowalczuk, P., Olszewski, J., Darecki, M., Kaczmarek, S., 2005. Empirical relationships between Coloured Dissolved Organic Matter (CDOM) absorption and apparent optical properties in Baltic Sea waters. International Journal of Remote Sensing 26, 345–370.

Lahet, F., Forget, P., Ouillon, S., 2001a. Application of a colour classification method to quantify the constituents of coastal waters from in situ reflectances sampled at satellite sensor wavebands. International Journal of Remote Sensing 22, 909–914.

Lahet, F., Ouillon, S., Forget, P., 2001b. Colour classification of coastal waters of the Ebro river plume from spectral reflectances. International Journal of Remote Sensing 22, 1639–1664.

Lee, Z.P., Carder, K.L., Steward, R.G., Peacock, T.G., Davis, C.O., Patch, J.S., 1998. An empirical algorithm for light absorption by ocean water based on color. Journal of Geophysical Research 103, 27967–27978.

Mallin, M.A., Burkholder, J.M., Cahoon, L.B., Posey, M.H., 2000. North and South Carolina Coast. Marine Pollution Bulletin 41, 56–75.

Maritorena, S., Siegel, D.A., Peterson, A.R., 2002. Optimization of semi-analytical ocean color model for global-scale applications. Applied Optics 41, 2705–2714.

Mitchell, B.G., 1994. Coastal zone color scanner retrospective. Journal of Geophysical Research 99, 7291–7292.

Mobley, C.D., 1994. Light and Water: Radiative Transfer in Natural Waters. Academic Press, San Diego, CA, 592pp.

Mobley, C.D., 1999. Estimation of the remote-sensing reflectance from above-surface measurements. Applied Optics 36, 7442–7455.

Moore, T.S., Dowell, M.D., Campbell, J.M., 2000. Universally Tailored Optical Parameter Inversion Algorithm (UTOPIA) I: Global Classification. In: Steven, G., Ackleson (Eds.), Proceedings of Ocean Optics XV Conference, paper no. 1218, 9pp., Monte Carlo, Monaco, 16–20 October 2000.

Morel, A., Prieur, L., 1977. Analysis in variation of ocean color. Limnology and Oceanography 22, 709–722.

Morel, A., Gentili, B., 1991. Diffuse reflectance of oceanic waters. II Bidirectional aspects. Applied Optics 32, 6864–6879.

Morel, A., Gentili, B., 1993. Diffuse reflectance of oceanic shallow water: Its dependence on sun angle as influenced by the molecular scattering distribution. Applied Optics 30, 4427–4438.

Mueller, J.L., Austin, R.W., 1995. Ocean Optics Protocols for SeaWiFS Validation, Revision 1. In: Hooker, S.B., Firestone, E.R., Acker, J.G. (Eds.), NASA Technical Memorandum. 104566, Vol. 25. NASA Goddard Space Flight Center, Greenbelt, Maryland, p. 67.

Nelson, J.R., Guarda, S., 1995. Particulate and dissolved spectral absorption on the continental shelf of the southeastern United States. Journal of Geophysical Research 100, 8715–8732.

O'Reilly, J.E., Maritorena, S., Mitchell, B.G., Siegel, D.A., Carder, K.L., Garver, S.A., Kahru, M., McClain, C., 1998. Ocean color chlorophyll algorithm for SeaWiFS. Journal of Geophysical Research 103, 24937–24953.

O'Reilly, J.E., Maritorena, S., Siegel, D.A., O'Brien, M.C., Toole, D., Mitchell, B.G., Kahru, M., Chavez, F.P., Strutton, P., Cota, G.F., Hooker, S.B., McClain, C.R., Carder, K.L., Müller-Karger, F., Harding, L., Magnuson, A., Phinney, D., Moore, G.F., Aiken, J., Arrigo, K.R., Letelier, R., Culver, M., 2000. Ocean color chlorophyll algorithms for SeaWiFS, OC2, and OC4: Version 4. In: Hooker, S.B., Firestone, E.R. (Eds.), SeaWiFS Postlaunch Calibration and Validation Analyses, Part 3, NASA Technical Memorandum, 2000-206892, Vol. 11. NASA Goddard Space Center, Greenbelt, MD, pp. 9–27.

Olszewski, J., Sokólski, M., 1990. Elimination of surface background in the contactless sea investigations. Oceanologia 29, 213–221.

Olszewski, J., Kowalczuk, P., 2000. Sky glint correction in measurements of upward radiance above the sea surface. Oceanologia 42 (2), 251–262.

Ouillon, S., Petrenko, A.A., 2005. Above water measurements of reflectance and chlorophyll-*a* algorithms in the Gulf of Lions, NW Mediterranean Sea. Optics Express 13, 2531–2548.

Sathyendranath, S., Prieur, L., Morel, A., 1989. A three-component model of ocean colour and its application to remote sensing of phytoplankton pigments in coastal waters. International Journal of Remote Sensing 10, 1373–1394.

Sosik, H.M., Green, R.E., Pegau, W.S., Roesler, C.S., 2001. Temporal and vertical variability in optical properties of New England shelf waters during late summer and spring. Journal of Geophysical Research 106, 9455–9472.

Sturm, B., Zibordi, G., 2002. SeaWiFS atmospheric correction by an approximate model and vicarious calibration. International Journal of Remote Sensing 23, 489–501.

Welschmeyer, N.A., 1994. Fluorometric analysis of chlorophyll *a* in the presence of chlorophyll *b* and pheopigments. Limnology and Oceanography 39, 1985–1992.

Wood, P., Cunnigham, A., 2001. Ship-borne measurements of ocean colour: development of a CCD-based reflectance radiometer and trials on the longitudinal transect of the Atlantic Ocean. International Journal of Remote Sensing 22, 99–111.

Wren, P.A., Leonard, L.A., 2005. Sediment transport on the mid-continental shelf in Onslow Bay, North Carolina during Hurricane Isabel. Estuarine, Coastal and Shelf Science 63, 43–56.

Zibordi, G., Berthon, J.F., 2001. Relationship between the Q-factor and seawater optical properties in a coastal region. Limnology and Oceanography 46 (5), 1130–1140.

Zibordi, G., Hooker, S.B., Berthon, J.F., D'Alimonte, D., 2002. Autonomous above-water radiance measurements from offshore platform: A field experiment. Journal of Atmospheric and Ocean Technology 19, 808–819.